X-ray Crystal Structures of the S229A Mutant and Wild-Type MurB in the Presence of the Substrate Enolpyruvyl-UDP-*N*-Acetylglucosamine at 1.8-Å Resolution[†,‡]

Timothy E. Benson, Christopher T. Walsh,* and James M. Hogle

Department of Biological Chemistry and Molecular Pharmacology, Harvard Medical School, 240 Longwood Avenue, Boston, Massachusetts 02115

Received August 30, 1996[⊗]

ABSTRACT: MurB catalyzes the second committed step in the synthesis of peptidoglycan, a key component of the bacterial cell wall. The crystal structures of both a S229A mutant and wild-type MurB in the presence of the substrate enolpyruvyl-UDP-*N*-acetylglucosamine were solved and refined at 1.8 Å resolution. The single point mutation of residue 229 from serine to alanine eliminated a hydroxyl group which has previously been proposed to play a critical role as a proton donor during the second half-reaction of MurB, namely, reoxidation of $FADH_2$ and reduction of the enolpyruvyl substrate. The mutation also resulted in the loss of the water molecule-hydrogen bonded to the serine hydroxyl in the wild-type structure changing the hydrogen-bonding network with in the active site. Comparison of the wild-type and S229A mutant structures confirms that the dramatic kinetic defect of an approximately 10^7-fold decrease observed for the Ser 229 Ala mutant in the second half-reaction [Benson, T. E., Walsh, C. T., & Massey, V. (1997) *Biochemistry 36*, 796−805] is a direct result of the loss of the serine hydroxyl moiety rather than other nonspecific active-site changes or general structural defects.

Cell wall biosynthesis in bacteria involves the assembly of a biopolymer called peptidoglycan which forms a cross-linked web outside the inner membrane of the cell. Peptidoglycan, with peptide and glycan strands linked via lactyl ether connecting units, serves as a critical structural unit of the cell wall by maintaining the osmotic integrity of the cell. The biosynthesis of peptidoglycan proceeds from UDP-*N*-acetylglucosamine with the two step synthesis of UDP-*N*-acetylmuramic acid catalyzed by the enzymes MurA and MurB (Bugg & Walsh, 1993) (Figure 1). MurA facilitates the addition of an enolpyruvyl moiety from phosphoenolpyruvate to the 3′ hydroxyl of UDP-*N*-acetylglucosamine (Gunetileke & Anwar, 1966). MurB is responsible for the reduction of the enol ether to the lactyl ether, utilizing 1 equiv of NADPH and a solvent-derived proton (Taku et al., 1970).

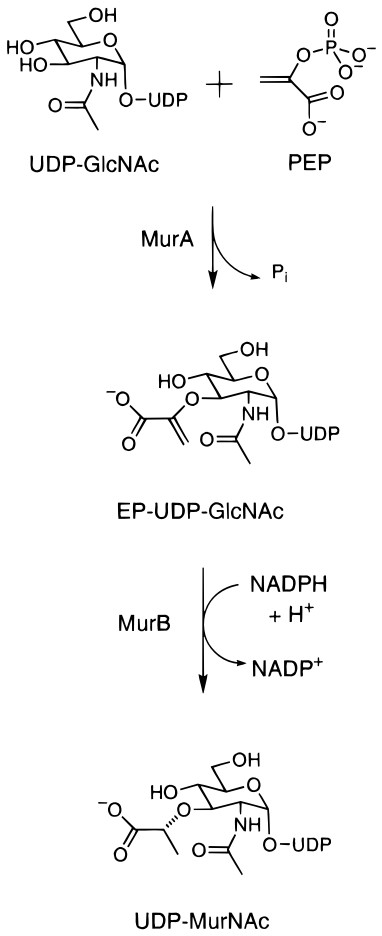

FIGURE 1: Biosynthetic pathway of UDP-*N*-acetylmuramic acid by the sequential action of the enzymes MurA and MurB.

Previous studies of MurB have focused on both the mechanistic and structural features of this flavoprotein during

[†] This work was supported in part by National Institutes of Health Grant GM49338 (C.T.W.) and the W. M. Keck Foundation (J.M.H.).

[‡] The coordinates for the S229A mutant and wild-type Mur B structures have been deposited in the Brookhaven Protein Data Bank. The ID code for the wild-type 1.8-Å structure is 2MBR and the ID code for the S229A structure is 1UXY.

[⊗] Abstract published in *Advance ACS Abstracts,* January 15, 1997.

[1] Abbreviations: (*E*)-EB-UDP-GlcNAc, uridine 5′-(trihydrogen diphosphate), *P*′-[2-(acetylamino)-3-*O*-[(*E*)-1-carboxyprop-1-enyl]-2-deoxy-α-D-glucopyranosyl] ester; (*Z*)-EB-UDP-GlcNAc, uridine 5′-(trihydrogen diphosphate), *P*′-[2-(acetylamino)-3-*O*-[(*Z*)-1-carboxyprop-1-enyl]-2-deoxy-α-D-glucopyranosyl] ester; FAD, flavin adenine dinucleotide; EP-UDP-GlcNAc, uridine 5′-(trihydrogen diphosphate), *P*′-[2-(acetylamino)-3-*O*-[(*E*)-1-carboxyeth-1-enyl]-2-deoxy-α-D-glucopyranosyl] ester; HEPES, (4-[2-hydroxyethyl]-1-piperazineethanesulfonic acid); $NADP^+$, oxidized β-nicotinamide adenine dinucleotide phosphate; NADPH, reduced β-nicotinamide dinucleotide phosphate; PEP, phosphoenolpyruvate; UDP-Me-MurNAc, uridine 5′-(trihydrogen diphosphate), *P*′-[2-(acetylamino)-3-*O*-(1-*R*-carboxypropyl)-2-deoxy-α-D-glucopyranosyl] ester; UDP-MurNAc, uridine 5′-(trihydrogen diphosphate), *P*′-[2-(acetylamino)-3-*O*-(1-*R*-carboxyethyl)-2-deoxy-α-D-glucopyranosyl] ester.

S0006-2960(96)02221-0 CCC: $14.00

FIGURE 2: Secondary structure representation of the wild-type MurB structure in complex with EP-UDP-GlcNAc. The flavin adenine cofactor and EP-UDP-GlcNAc substrate are shown as stick models. The coordinates from the refined 1.8-Å structure were used to generate this figure using Molscript (Kraulis, 1991).

its reduction of enolpyruvyl-UDP-*N*-acetylglucosamine (EP-UDP-GlcNAc).[1] In an earlier publication we reported the structure of the wild-type enzyme as a complex with the EP-UDP-GlcNAc substrate at 2.7-Å resolution (Benson et al., 1995) (see Figure 2). The structure revealed a clear architecture for the reduction of the enol ether. The bound EP-UDP-GlcNAc was ideally positioned below the flavin adenine dinucleotide (FAD) with N5 of the FAD, the locus of hydride transfer, directly above C3 of the enolpyruvyl moiety, the locus of hydride addition as identified during earlier mechanistic studies (Benson et al., 1993). Two residues, Glu 325 and Arg 159, were suitably situated to stabilize the developing carbanion at C2 of the enolpyruvate by providing a hydrogen bond to generate an enol rather than enolate intermediate. A third active-site residue, Ser 229, was in prime position to serve as a proton donor to quench the carbanion and complete the reduction (Benson et al., 1995).

The proposed role of Ser 229 was particularly unusual as the pK_a (~13−15) of the serine hydroxyl does not favor its role as a proton donor in most enzymatic reactions. Therefore, we sought to further investigate the role of this residue through mutational analysis. By mutating serine 229 to alanine, we hoped to create a mutant enzyme able to support the first half-reaction, namely, the reduction of FAD by NADPH, but specifically defective in the second half-reaction, the reoxidation of $FADH_2$ and coordinate reduction of EP-UDP-GlcNAc. The accompanying paper (Benson et al., 1997) describes the successful engineering of the Ser 229 Ala mutant which, in fact, was competent to complete the first half-reaction yet was dramatically impaired in its ability to complete the second half-reaction. This study,

Table 1: Data Collection Statistics for Wild-Type MurB by Resolution Shells

	resolution bins (Å)								
	20.00−3.59	2.86	2.50	2.27	2.10	1.98	1.88	1.80	all data
R_{sym}[a]	0.032	0.036	0.041	0.049	0.064	0.084	0.117	0.157	0.042
unique reflections	4184	3904	3839	3755	3589	3385	3211	2962	28,829
$\langle I/\sigma \rangle$	51.8	43.6	39.0	33.1	27.3	21.2	15.9	12.3	31.8
completeness (%)	97.5	97.6	98.1	96.1	93.0	88.6	98.6	77.3	91.6
multiplicity	9.3	7.6	7.9	7.4	7.1	6.8	6.6	6.4	7.5

[a] $R_{sym} = \sum_{i(h,k,l)} |I_{i(h,k,l)} - \langle I_{(h,k,l)} \rangle| / \sum_{i(h,k,l)} \langle I_{(h,k,l)} \rangle$, where $\langle I_{(h,k,l)} \rangle$ is the statistically weighted average intensity of symmetry-equivalent reflections.

Table 2: Data Collection Statistics for S229A MurB by Resolution Shells

	resolution bins (Å)								
	20.00−3.59	2.86	2.50	2.27	2.10	1.98	1.88	1.80	all data
R_{sym}[a]	0.027	0.031	0.041	0.055	0.077	0.098	0.144	0.181	0.041
unique reflections	4099	3912	3826	3799	3690	3506	3244	3066	29,142
$\langle I/\sigma \rangle$	41.3	38.7	31.6	25.3	19.7	15.1	10.8	8.13	24.8
completeness (%)	95.9	98.0	98.1	97.7	96.1	91.4	85.4	79.6	92.9
multiplicity	6.5	6.6	6.4	6.0	5.5	5.2	4.8	4.4	5.7

[a] R_{sym} is defined in Table 1.

Table 3: Refinement Statistics[a]

				rms deviations		
	R-factor[b]	free *R*-factor[c]	no. of reflections	bonds (Å)	angles (deg)	impropers (deg)
wild type	0.203	0.256	28 770	0.010	1.56	1.35
S229A	0.202	0.246	29 040	0.010	1.55	1.34

	average *B*-factors				
	main-chain atoms	side-chain atoms	waters	FAD	EP-UDP-GlcNAc
wild type	23.4	24.9	33.4	16.2	18.6
S229A	20.3	22.0	30.1	13.9	16.7

[a] Statistics are given for WT (2988 non-hydrogen atoms including 237 waters) and S229A MurB (2985 non-hydrogen atoms including 235 waters) from 20 to 1.8 Å including all data (no σ cutoff). [b] Crystallographic *R* factor = $\sum_{(h,k,l)} ||F_o| - |F_c|| / \sum_{(h,k,l)} |F_o|$. [c] Free *R* factor = $\sum_{(h,k,l) \in T} ||F_o| - |F_c|| / \sum_{(h,k,l) \in T} |F_o|$, where *T* is a test set containing a randomly selected 10% of the observations omitted from the refinement process.

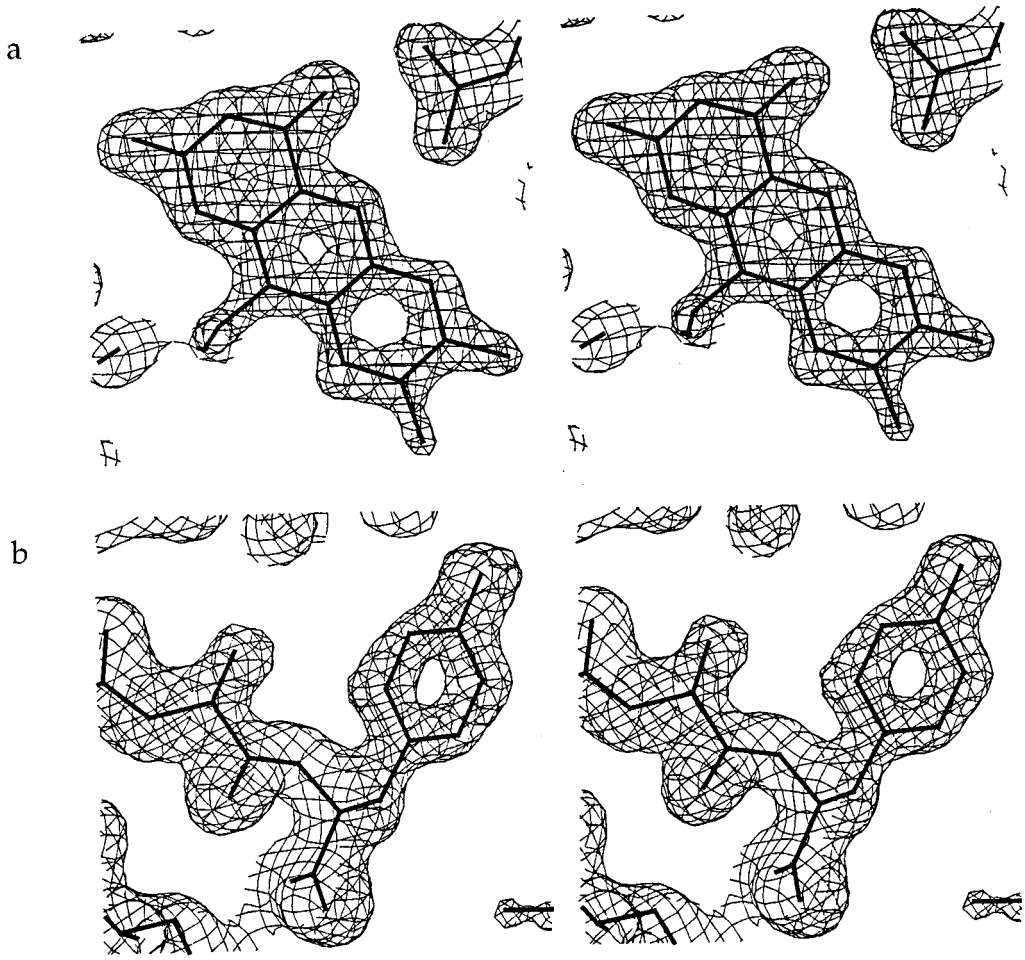

FIGURE 3: (a) Electron density for the FAD cofactor in the wild-type MurB structure at 1.8-Å resolution. This $2F_o - F_c$ map is contoured at 2.0σ. (b) Electron density for a portion of the main chain in the wild-type MurB structure from residues 123 to 125. This $2F_o - F_c$ map is contoured at 1.5σ. This figure was prepared using Setor (Evans, 1990).

which showed that the mutation results in an approximately 10^7-fold decrease in reoxidation rate observed for the S229A mutant and a significant biasing of catalysis in the mutant enzyme of the alternate substrate *(E)*-enolbutyryl-UDP-GlcNAc toward isomerization to (*Z*)-enolbutyryl-UDP-GlcNAc as opposed to reduction to give the product UDP-*N*-acetylmethylmuramic acid, provided biochemical evidence for the role of Ser 229 as the proposed proton donor in the wild-type enzyme.

In order to complete our studies of the Ser 229 Ala mutant we have solved and refined the structure of the mutant enzyme to 1.8-Å resolution. We have also extended the resolution of the wild-type enzyme structure from 2.7 to 1.8 Å. The higher resolution structure of the MurB-EP-UDP-GlcNAc complex increases the accuracy of the earlier model, providing a more precise definition of the positions of key residues and solvent molecules involved in catalysis and providing a more suitable model for the design of potential antibacterial agents. In addition, comparison of the high-resolution models of the wild type and S229A mutant provides key evidence that the loss of the serine hydroxyl is directly responsible for the striking alternations in the kinetic properties of the S229A mutant.

MATERIALS AND METHODS

Crystallization of S229A MurB. Crystals of S229A MurB were grown in 15−18% PEG 8000, 100 mM HEPES pH 8.0, 200 mM calcium acetate, and 7 mM EP-UDP-GlcNAc with a protein concentration of 10 mg/mL as described previously for wild-type enzyme (Benson et al., 1994). The crystals grew to a size of $0.2 \times 0.2 \times 0.3$ mm over a period of 2−3 days. S229A crystals belong to the same space group as wild-type crystals, $P4_32_12$, with unit cell constants $a = b = 49.2$ Å and $c = 261.8$ Å. Cell constants for the wild-type crystal used in data collection were $a = b = 49.3$ Å and $c = 262.5$ Å.

Data Collection. X-ray diffraction data were collected at the National Synchrotron Light Source at Brookhaven National Laboratory (Upton, NY) at beam line X12C. Data collection on single crystals was conducted at −170 °C under a stream of liquid nitrogen using an Oxford cryogenic system. Crystals were soaked in crystallization buffer plus 17% glycerol before mounting in the liquid nitrogen stream. Data were collected on a 30-cm Mar imaging detector (Mar Research) mounted on a 2θ axis. Diffraction data were collected at crystal to detector distances of 342−452 mm and 2θ settings between 0° and 21.5°.

Data Processing and Refinement. X-ray crystallographic data were indexed and integrated using the program DENZO (Otwinowski, 1993). Integrated reflections were scaled using the program SCALEPACK (Otwinowski, 1993). Data collection statistics for wild-type and S229A mutant MurB are shown in Tables 1 and 2, respectively. Structure factor amplitudes were calculated using TRUNCATE from the

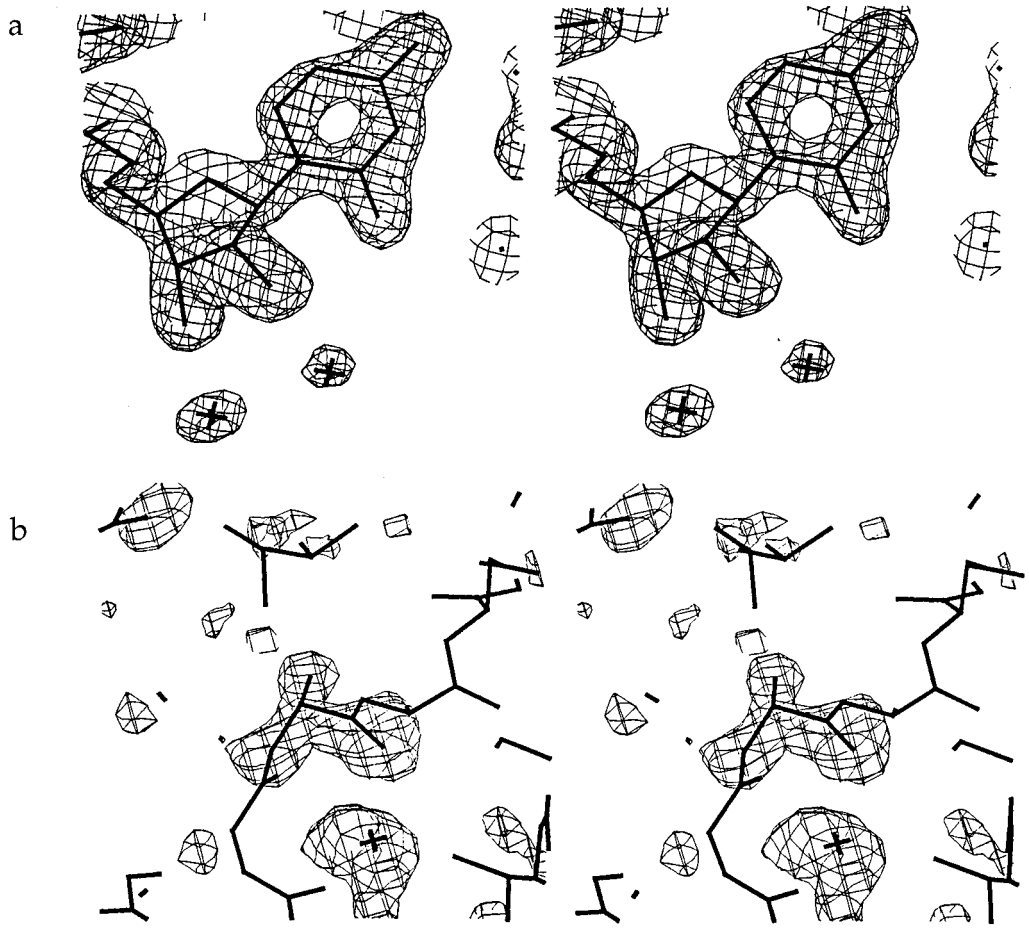

FIGURE 4: (a) Electron density for the EP-UDP-GlcNAc substrate from the S229A mutant MurB at 1.8-Å resolution. This $2F_o - F_c$ map is contoured at 1.5σ. (b) Positive electron density for residue 229 in the S229A mutant MurB at 1.8-Å resolution. This map was calculated after an initial round of energy minimization and simulated annealing using the wild-type model with residue 229 omitted from the refinement and map calculations. This $F_o - F_c$ map is contoured at 2.0σ. This figure was prepared using Setor (Evans, 1990).

CCP4 package (Collaborative Computational Project No. 4, 1994; French & Wilson, 1978). Before any refinement was conducted, a set of randomly chosen reflections comprising 10% of the total reflections was selected for the R_{free} test set for cross-validation of the model during refinement (Brünger, 1992a). This new test set included those reflections previously used as test reflections during the refinement to 2.7 Å.

The starting model used for the high-resolution refinement of the wild-type MurB structure was the 340 amino acid model plus the two ligands, EP-UDP-GlcNAc and FAD, previously refined to 2.7 Å (Benson et al., 1995). The starting model for the S229A mutant was the same as the wild-type model except that Ser 229 was omitted. The water structure was entirely rebuilt for both structures to avoid biasing the water model toward poorly built waters at lower resolution. Refinement began with one round of rigid-body refinement followed by energy minimization and *B*-factor refinement using X-PLOR (Brünger, 1992b). Subsequent rounds of refinement included a bulk solvent correction (including a single scale and *B*-factor) to more accurately model the diffuse solvent at the border of the protein (Jiang & Brünger, 1994), followed by overall anisotropic *B*-factor refinement, energy minimization, simulated annealing, and individual *B*-factor refinement. After each round of simulated annealing, each residue was checked against $2F_o - F_c$ and $F_o - F_c$ maps for correct placement of main-chain and side-chain atoms. Side chains at the surface of the molecule for which there was no visible electron density were modeled with occupancies and *B*-factors were set to 0. Waters were built into the structure when there was spherically shaped electron density present in both the $2F_o - F_c$ and $F_o - F_c$ maps with reasonable hydrogen-bonding partners. Waters were only kept in the model if their refined *B*-factors were below 50 Å^2. Refinement statistics for both structures are shown in Table 3.

RESULTS AND DISCUSSION

Electron density maps for the wild-type MurB showed visible improvement over previous lower resolution maps. The maps for the S229A mutant were of comparable high quality. Main-chain nitrogens, α carbons, and carbonyl oxygens were generally well-defined. Side-chain density was clear for over 98% of the residues. Sample electron density maps from both wild-type and S229A MurB are shown in Figures 3a,b and 4a exemplifying densities for the FAD cofactor, main-chain and side-chain atoms, and the EP-UDP-GlcNAc substrate. Comparison of the high-resolution wild-type and mutant structures shows a high degree of overall similarity. The rms deviation for the two structures (excluding solvent molecules) for all atoms is 0.4 Å and for main-chain atoms alone is 0.2 Å. Significant main-chain differences between the two structures are restricted to two short loops between residues 144 and 147 and between residues 256 and 259 where the electron density is not well-defined.

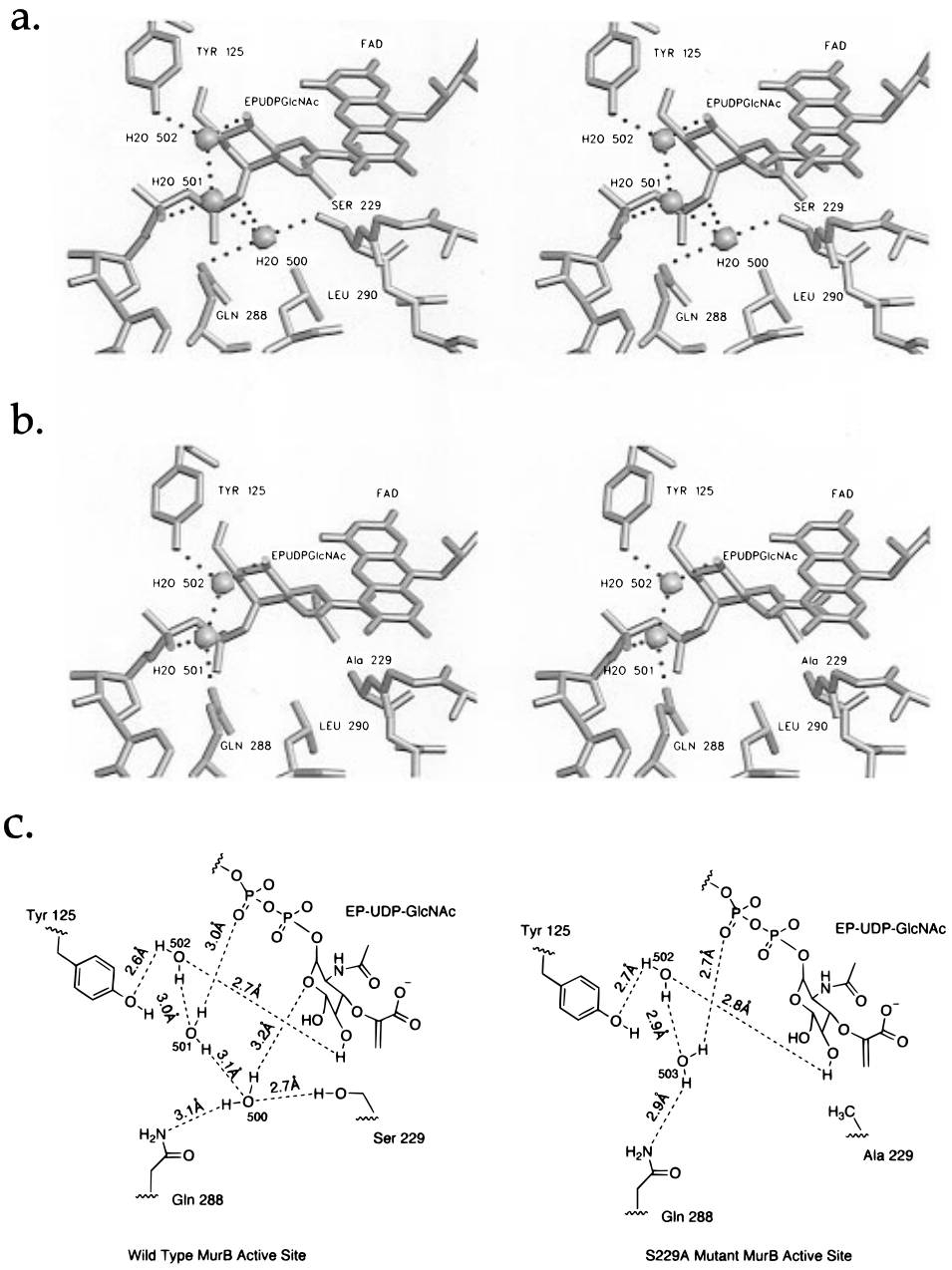

FIGURE 5: Stereoviews of the active sites of both the S229A MurB mutant and wild-type MurB. (a) The active site of wild-type MurB showing the three active-site waters critical for supporting the protonation of C2 by Ser 229. (b) The active site of S229A showing the rearranged hydrogen-bonding network as a result of the movement of Wat 501. The loss of the serine hydroxyl moiety destabilizes the hydrogen-bonding network for Wat 500 found in the wild-type structure leading to the mutant's inability to support this water within the active site. (c) Schematic views of the wild-type and S229A mutant active sites with hydrogen-bonding distances shown in angstroms. Panels a and b were prepared using Setor (Evans, 1990).

The most significant observations pertaining to mechanism for both the wild-type and mutant structures occur within the active site. The active site of wild-type MurB with EP-UDP-GlcNAc bound reveals the same architecture for hydride transfer from N5 of the FAD to C3 of EP-UDP-GlcNAc at 1.8-Å resolution as it did at 2.7-Å resolution. The distance between N5 and C3 is 3.1 Å in the high-resolution structure, well within the range for hydride transfer. Similarly, O1A and O1B of Glu 325 and Nη2 of Arg 159 are positioned within hydrogen-bonding range (2.8−3.2 Å) of O1B of EP-UDP-GlcNAc The coordination of Wat 605 does not include O1B of EP-UDP-GlcNAc as previously observed.

As observed in the 2.7-Å structure, the Ser 229 hydroxyl is 3.1 Å away from C2, suitably poised for proton addition to the C2 carbanion transition state as the D-lactyl ether product is formed in the MurB active site. Likewise, an important active-site water, Wat 500, in the 1.8-Å structure is coordinated by Ser 229, NE2 of Gln 288, Wat 501, and O1 of EP-UDP-GlcNAc. Wat 500 remains 4.5 Å away from C2, suggesting that its participation in substrate C2 carbanion protonation could only occur indirectly through Ser 229. Wat 501 and Wat 502 complete an important network of hydrogen bonds within the active site. Wat 501 provides a fourth, stabilizing coordination partner for Wat 500 while Wat 502 assists in the coordination of Wat 501. The hydrogen-bonding network for the wild-type active site is shown in Figure 5a, with explicit distance measurements shown in Figure 5c.

During the first round of refinement for the S229A mutant structure, residue 229 was omitted. The difference map from this refinement cycle showed clear positive electron density within the active site consistent with the identity of residue 229 as an alanine (Figure 4b). The loss of the serine hydroxyl does not result in significant changes in the positions of the protein atoms in the active site of the S229A mutant (rms deviation for all atoms including ligands within the active site is 0.2 Å). However, the loss of the serine hydroxyl does result in significant disruption the hydrogen-bonding network previously observed in the wild-type structure within the active site. In particular, the absence of the serine hydroxyl leads to the inability of the active site to support the presence of Wat 500 (Figure 5b,c). The adjacent water, Wat 501, now utilizes NE2 of Gln 288 as a coordination partner in the absence of its former coordination with Wat 500.

The virtual elimination of the ability of S229A MurB to complete the reduction of EP-UDP-GlcNAc (Benson et al., 1997) points to a pivotal role for the serine 229 hydroxyl during normal catalysis. The minimal changes in the structure of the S229A mutant enzyme as a whole compared to the wild-type enzyme and in particular the minimal changes within the active site of the two structures strongly support a model in which the decreased ability to catalyze the second half-reaction is directly due to the absence of the hydroxyl oxygen and its water partner, Wat 500, rather than a secondary effect and therefore support the proposed role of Ser 229 as a general acid. The absence of Wat 500 leads us to view serine 229 and the adjacent water as a catalytic pair which serve to protonate C2 of the enolpyruvyl-UDP-*N*-acetylglucosamine [see Figure 10 of the accompanying paper (Benson et al., (1997)]. The location of the serine hydroxyl within 3.1 Å of C2, the locus of protonation, points toward the hydroxyl moiety playing the interactive role in completing the reduction of the enolpyruvate while the adjacent water serves as a proton relay to reprotonate the serine. The active site of the S229A mutant reveals that the loss of a single hydrogen-bond donor/acceptor (the serine hydroxyl) disrupts the critical network of supporting hydrogen bonds necessary for normal catalysis and leads to approximately a 9.8 kcal/mol increase in the energy barrier for protonation of the nascent product carbanion that follows the $FADH_2$ reoxidation/hydride transfer step.

ACKNOWLEDGMENT

We thank Robert M. Sweet, Michelle W. Wien, and Harmon Zuccola for valuable assistance during synchrotron data collection at the National Synchrotron Light Source, Beamline X12C.

REFERENCES

Benson, T. E., Marquardt, J. L., Marquardt, A. C., Etzkorn, F. A., & Walsh, C. T. (1993) *Biochemistry 32*, 2024−2030.
Benson, T. E., Walsh, C. T., & Hogle, J. M. (1994) *Protein Sci. 3*, 1125−1127.
Benson, T. E., Filman, D. J., Walsh, C. T., & Hogle, J. M. (1995) *Nature Struct. Biol. 2*, 644−653.
Benson, T. E., Walsh, C. T., & Massey, V. (1997) *Biochemistry 36*, 796−805.
Brünger, A. T. (1992a) *Nature 355*, 472−475.
Brünger, A. T. (1992b) *X-PLOR Version 3.1: A System for X-ray Crystallography and NMR*, Yale University Press, New Haven.
Bugg, T. D. H., & Walsh, C. T. (1993) *Nat. Prod. Rep.* 199−215.
Collaborative Computational Project No. 4 (1994) *Acta Crystallogr. D50*, 760−763.
Evans, S. V. (1990) *J. Mol. Graphics 11*, 134−138.
French, G. S., & Wilson, K. S. (1978) *Acta Crystallogr. A34*, 517−525.
Gunetileke, K. G., & Anwar, R. A. (1966) *J. Biol. Chem. 241*, 5740−5743.
Jiang, J.-S., & Brünger, A. T. (1994) *J. Mol. Biol. 243*, 100−115.
Kraulis, P. J. (1991) *J. Appl. Crystallogr. 24*, 946−950.
Otwinowski, Z. (1993) in *Data Collection and Processing* (Sawyer, L., Isaacs, N., & Bailey, S., Eds.) pp 56−62, SERC Daresbury Laboratory, Warrington, England.
Taku, A., Guntileke, K. G., & Anwar, R. A. (1970) *J. Biol. Chem. 245*, 5012−5016.

BI962221G